Received: 14 August 2017 | Revised: 26 December 2017 | Accepted: 2 February 2018

DOI: 10.1002/cnm.2966

RESEARCH ARTICLE - FUNDAMENTAL

WILEY

Effects of fibroblast-myocyte coupling on the sinoatrial node activity: A computational study

Alexey A. Karpaev[1] | Roman A. Syunyaev[1] | Rubin R. Aliev[1,2]

[1]Moscow Institute of Physics and Technology, 141700 Dolgoprudny, Russia

[2]Institute of Theoretical and Experimental Biophysics, 142290 Puschino, Russia

Correspondence
Rubin R. Aliev, Institute of Theoretical and Experimental Biophysics, 142290 Puschino, Russia.
Email: rubaliev@gmail.com

Abstract

While the sinoatrial node (SAN) is structurally heterogeneous, most computer simulations of electrical activity take into account SAN pacemaker cells only. Our aim was to investigate how fibroblasts affect the SAN activity. We simulated the rabbit sinoatrial node accounting for differences between central and peripheral pacemaker cells, and for fibroblast-myocyte electrical coupling. We have observed that only if fibroblast-myocyte coupling is taken into account, (1) action potential is initiated in the central part of the SAN (within 1.2 mm of the center of simulated tissue); otherwise, leading centers are located on the periphery; (2) few (1 to 6) leading centers initiate action potential in the SAN; otherwise, we observed more than 8 leading centers; (3) acetylcholine superfusion results in a shift of leading centers toward the SAN periphery; and (4) sinus pauses up to 1.9 second follow acetylcholine superfusion. We observed negligible effect of fibroblast-myocyte coupling on the period of SAN activation. We conclude that fibroblast-myocyte coupling may explain action potential initiation and propagation from the center of the SAN observed in experimental studies, while atrial load on the peripheral SAN fails to explain this fact.

KEYWORDS

fibroblasts, leading center, mathematical model, pacemaker, sinoatrial node

1 | INTRODUCTION

The sinoatrial node (SAN), a natural pacemaker of the heart, is a heterogeneous structure composed of different types of cells including pacemaker cells, atrial cells, and fibroblasts.[1,2] Pacemaker cells, the major type of the SAN cells, differ in properties: Smaller cells with slow intrinsic pacing rate are mostly located in the center, while larger faster-oscillating ones are on the periphery.[1] The distribution of cells in the SAN poses a problem: Leading centers (LCs), where action potential is initiated and starts to propagate, are expected on the periphery of the SAN because the fastest oscillator generally suppresses slower ones. However, many experimental observations demonstrate propagation from the center to the periphery.[1] The dynamics is ordinarily explained by an electronic load imposed by an atrium: Coupling of atrial cells to SAN pacemaker cells may slow down or even suppress spontaneous activity of SAN pacemakers.[3,4] This may result in a shift of LCs toward the center of the SAN. However, computer simulations show that extremely high conductance is required to shift the LC to the proper position: eg, 37.5 nS intercellular conductance in the center and 375 nS on the periphery of the SAN,[5] while experimental observations of the value range from 0.6 to 25 nS.[6] Experimental observations in the rabbit SAN[1,26] also show that an LC is not fixed but shifts by few millimeters toward the SAN periphery in

response to a physiological stimulus such as acetylcholine (ACh) superfusion. Below, we consider if central location of LCs, as well as their shift induced by ACh, is feasible without an assumption of extreme intercellular conductances, but with an account of SAN nonpacemaker cells. An excellent introduction to the problem may be found in the reviews by Boyett and Mangoni.[1,7]

Sinoatrial node tissue contains various types of cells, among which fibroblasts occupy 45 to 75% of the SAN.[8-10] Fibroblasts are shown to couple electrically to pacemaker cells in vivo,[11,12] and to myocytes in cultured tissues.[13,14] Gap junction connexins Cx43 and Cx45 were found between myocytes and fibroblasts in neonatal rat ventricles in vivo.[15] The role and the effect of fibroblast-myocyte coupling on electrical activity of the SAN open novel fields to study. Computer simulations of isolated SAN cells coupled to fibroblasts show pronounced reduction of central SAN cell cycle length (CL) and action potential amplitude, while peripheral cells' action potential changes were relatively weak.[16] Here, we present results of detailed computer simulations of SAN electrical activity affected by fibroblasts.

2 | METHODS

2.1 | Ionic models

To simulate electric activity of the SAN, we have exploited the ionic model of the rabbit SAN pacemaker cells described earlier in Aliev and Chailakhyan, Aliev et al, and Zhang et al[17-21]; full set of equations in Aliev[22]; and supporting information; accounting for 15 ionic currents, intracellular ionic concentration changes, and sarcoplasmic reticulum function:

$$-C_{\mathrm{m}}\frac{dE_{\mathrm{SAN}}}{dt} = I_{\mathrm{Na}} + I_{\mathrm{CaL}} + I_{\mathrm{CaT}} + I_f + I_{\mathrm{Kr}} + I_{\mathrm{Ks}} + I_{\mathrm{to}} + I_{\mathrm{sus}} + I_{\mathrm{KACh}} + I_{\mathrm{bNa}} + I_{\mathrm{bCa}} + \\ + I_{\mathrm{bK}} + I_{\mathrm{NaK}} + I_{\mathrm{NaCa}} + I_{\mathrm{Cap}} \tag{1}$$

where I_{Na} is fast sodium current; I_{CaL} is L-type calcium current; I_{CaT} is T-type calcium current; I_f is depolarization activated current; I_{Kr} is rapid potassium current; I_{Ks} is slow potassium current; I_{to} and I_{sus} are 4 aminopyridine sensitive currents; I_{KACh} is ACh-dependent potassium current; I_{bNa}, I_{bK}, and I_{bCa} are background currents; I_{NaK} is sodium-potassium pump current; I_{NaCa} is sodium-calcium exchanger current; and I_{CaP} is calcium pump current.

To simulate atrial cells' action potential, we used Lindblad et al model.[23]

$$-C_{\mathrm{m}}\frac{dE_{\mathrm{AT}}}{dt} = I_{\mathrm{Na}} + I_{\mathrm{CaL}} + I_{\mathrm{CaT}} + I_{\mathrm{K1}} + I_{\mathrm{Kr}} + I_{\mathrm{Ks}} + I_{\mathrm{to}} + I_{\mathrm{bNa}} + I_{\mathrm{bCa}} + \\ + I_{\mathrm{bCl}} + I_{\mathrm{NaK}} + I_{\mathrm{NaCa}} + I_{\mathrm{Ca,p}} \tag{2}$$

where I_{bCl} is background chloride current and I_{K1} is inner rectifying potassium current, other currents as above. The model was chosen because it is mostly based on voltage-clamp data from rabbit atrial myocytes and provides morphological features of rabbit atrial action potential.

To simulate fibroblast electrical activity, we used MacCannell et al model that accounted for delayed-rectifier potassium current (I_{Kv}), inward-rectifying potassium current (I_{K1}), sodium-potassium exchanger (I_{NaK}), and background sodium currents ($I_{\mathrm{b,Na}}$) (the full set of equations is in MacCannell et al[24] and in the supporting information):

$$-C_{\mathrm{m,fb}}\frac{dE_{\mathrm{fb}}}{dt} = I_{\mathrm{K_v}} + I_{\mathrm{K1}} + I_{\mathrm{NaK}} + I_{\mathrm{b,Na}} \tag{3}$$

We have simulated the mesh of cells interconnected via gap junctions, which was described by the system of ordinary differential equations:

$$\begin{cases} -C_{\mathrm{m}}\dfrac{dE_i}{dt} = \sum\limits_i I^{(i)} + \sum\limits_j g_{\mathrm{gap,myo}}\left(E_i - E_j\right) + \sum\limits_k g_{\mathrm{gap,fb}}\left(E - E_{\mathrm{fb_k}}\right) \\ -C_{\mathrm{m,fb}}\dfrac{dE_{\mathrm{fb}}}{dt} = \sum\limits_i I_{\mathrm{fb}^{(i)}} + g_{\mathrm{gap,fb}}\left(E_{\mathrm{fb}} - E\right) \end{cases} \tag{4}$$

where C_{m} is the membrane capacitance of SAN cells, $C_{\mathrm{m,\ fb}}$ is the membrane capacitance of fibroblasts, E_i is the membrane potential of ith cardiomyocyte, E_j is the membrane potential of cardiomyocytes surrounding ith

cardiomyocyte, E_{fb} is the membrane potential of fibroblasts, $I^{(i)}$ are currents in myocytes, $I_{fb^{(i)}}$ are currents in fibroblasts, and $g_{gap,\ myo}$, $g_{gap,\ fb}$ are gap-junction conductivities (60 nS between the SAN cells, 88 nS between the SAN and atrial cells, 175 nS between atrial cells,[25] and 3 nS between fibroblasts and the SAN cells[26]).

The effect of ACh was simulated by inhibition of L-type calcium currents, activation of ACh-dependent potassium current, and shift of the activation curve of the hyperpolarization-activated current.[21] We used 60-nmol/L ACh as this concentration is high enough to severely slow down pacing rate of the SAN cells, while still not high enough to suppress spontaneous activity. Dose-response curves observed in a similar model may be found in Boyett et al.[28]

We have accounted for differences between cells of the SAN central and peripheral type[20] as well as intermediate cells, whose parameters were interpolated as $p(\mathrm{ct}) = p_c + \mathrm{ct} * p_p$, where ct is the cell type index, varied from 0 to 1; p_c and p_p are the values of parameters corresponding to central and peripheral pacemakers.[29] In other words, ct = 0 corresponds to central cells and ct = 1 corresponds to peripheral cells.

2.2 | SAN geometry

In simulations, the tissue consisted of 200 × 200 70-μm-long myocardial cells (Figure 1A); ie, spatial step was equal to the cell size. Sinoatrial node cells of different types were placed randomly within the SAN area according to the normal distribution:

$$f(\mathrm{ct}) = \frac{1}{\sigma\sqrt{2\pi}} \cdot \exp\left(-\frac{\left(\mathrm{ct} - {}^{r}/_{R_{SAN}}\right)^2}{2\sigma^2}\right) \tag{5}$$

where f is the probability density function, ct is the cell type index, r is the distance to the center of the SAN, $R_{SAN} = 4900$ μm is the distance from the center to the SAN boundary, and $\sigma = 0.6$ is the standard deviation. Thus, cells of central, peripheral, and intermediate types were distributed in a random manner; however, the probability density function was maximal for central type cells in the center of the SAN and for peripheral type cells near the SAN periphery. The SAN area was surrounded by a transitional area where SAN cells were intermingled with atrial cells. The probability of SAN cells to occur at a distance $R_{SAN} < r < R_{AT}$ from the center in transitional area was

$$P_{tr} = 2\int_0^{\frac{R_{AT}-r}{R_{AT}-R_{SAN}}} \frac{1}{\sigma_T\sqrt{2\pi}} \cdot e^{-\frac{x^2}{2\cdot\sigma_T{}^2}} dx \tag{6}$$

where $\sigma_T = 0.7$, $R_{AT} = 6300\,\mu$m. The transitional area itself was surrounded by atrial cells. This description can be regarded as a model intermediate between "gradient" and "mosaic" models of the SAN structural organization, which was used previously in Syunyaev and Aliev.[30] According to the "gradient" model, there is a progressive transition of the SAN cell properties from the SAN center to periphery, while according to the "mosaic" model, central and peripheral SAN cells are uniformly distributed within the SAN; however, atrial cells are more common on the SAN periphery (see also Mangoni and Nargeot[7] on gradient and mosaic models).

In this work, we used a 2D circular geometry of the SAN with 70-μm-long square myocardial cells, which is equivalent, for example, to the elliptical SAN 7 mm long and 1.4 mm wide if to consider 50 × 10-μm prolonged cells oriented in parallel to the *crista terminalis*. As a matter of fact, there is no preferential orientation of myocytes at least within the central SAN region: The SAN cells form rather irregular mesh.[31] The particular effects of the SAN geometry and fiber orientation were not the purpose of this study; our focus was on principal effects of fibroblasts on the SAN activation. Thus, we kept the model as simple as possible to outline the discussed phenomena; simulations with a simplified geometry allowed us to simplify the data analysis and to concentrate on the observed effects. Simulations with the accurate SAN geometry based on the data from Dobrzynski et al[31] are provided below for comparison and were carried out as described previously.[30]

Previously, Xie et al[32] proposed a 2D model of ventricular tissue that can be visualized as 2 interacting sheets: a layer of fibroblasts over a layer of myocytes. They used the fibroblast size of 25 × 25 × 25 μm and myocyte size of 125 × 25 × 25 μm; thus, 1 myocyte could interact with several (up to 5) fibroblasts. We used the same approach here; however, SAN cells are smaller than ventricular cells, and therefore, the number of fibroblasts coupled to single SAN cells was ranged from 0 to 3 in simulations (Figure 1B): Every SAN cell was adjacent to 3 "sites," each of which could

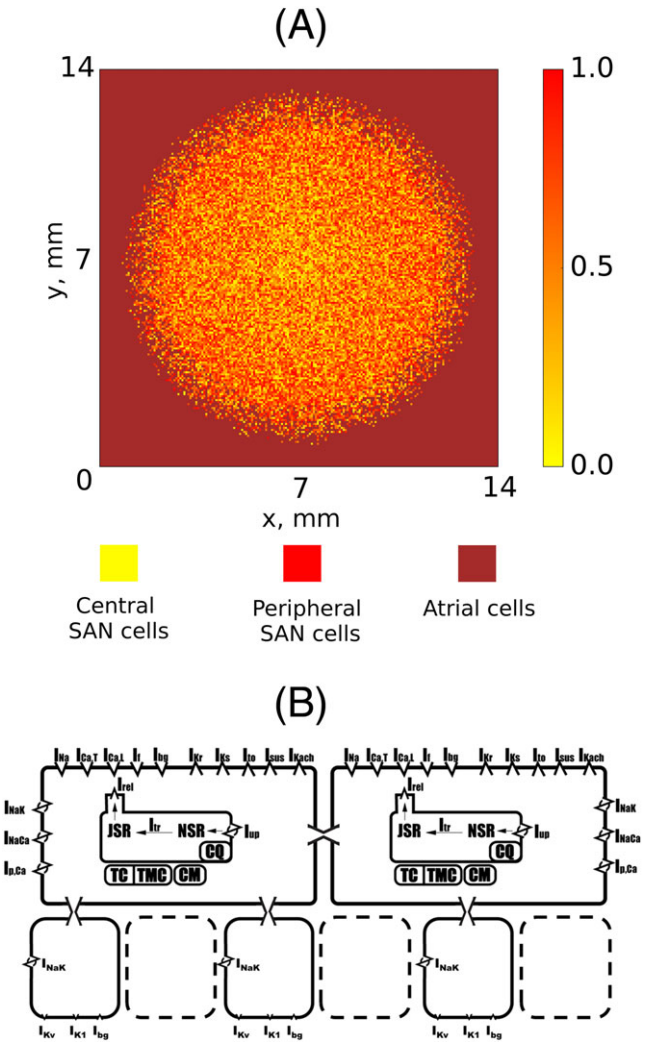

FIGURE 1 A, Sinoatrial node (SAN) geometry used in simulations. SAN cell-type indexes stand: 0.0 for central cells, tinted yellow; 1.0 for peripheral cells, tinted red; see the color bar for intermediate types. Atrial cells are brown. B, A scheme of pacemaker cells coupled to fibroblasts. As an example, the left SAN cell is coupled to 2 fibroblasts, the right one to a single fibroblast. Each cell may be coupled to up to 3 fibroblasts (vacant fibroblast "sites" are depicted by a dashed line; see text for explanations). JSR, NSR-junctional sarcoplasmic reticulum, network sarcoplasmic reticulum correspondingly; TC, TMC-calcium and magnesium binding troponin sites; CM, CQ-calmodulin and calsequestrin correspondingly

be either vacant or filled by a fibroblast. The probability, P, of a site to be occupied by a fibroblast was varied from .0 to.6. $P = .0$ corresponds to simulations without fibroblast-myocyte coupling, ie, in the absence of fibroblasts. $P > 0$ corresponds to simulations accounting for fibroblast-myocyte coupling, ie, in the presence of fibroblasts.

The ACh effects as well as fibroblast-myocyte coupling were limited to the SAN area only. The former is justified by the fact that parasympathetic innervation of atrial tissue is minor compared with the SAN[33,34]: The density of parasympathetic innervation was estimated to be 6.8-fold higher in the intercaval region in comparison with *crista terminalis* region.[33] The latter is because no fibroblast-myocyte coupling was reported in atrial tissue in vivo.[12]

2.3 | Simulation protocols and techniques

Cells were distributed in the SAN as described above. To study the effect of fibroblast-myocyte coupling, we used the same cell distribution in all simulations and varied the number of fibroblasts coupled to myocytes. We used a uniform distribution of phase of oscillations as initial conditions[4,35] in all simulations. We simulated each case for 60 seconds without ACh followed by 60 seconds in the presence of 60 nmol/L of ACh.

An explicit Euler method with the time step of 0.01 ms was used, while Rush-Larsen method[36] was used in ionic current gate equations to improve stability. Simulations were encoded in C/MPI and run on INM RAS cluster. Each run took about 12 hours on 16 Intel Xeon X5650 6-core CPUs.

2.4 | Analysis and definitions

In this work, we consider a cell to be an LC if its activation time $t_{E=-30\ mV}$ was earlier than that of neighboring cells within a sphere of 210-μm radius. To estimate the activation time in the case of almost simultaneous depolarization, a linear interpolation was used:

$$t_{E=-30\ mV} = t + \frac{-30-E(t)}{E(t+\Delta t)-E(t)}\Delta t \tag{7}$$

Cycle length was calculated as the difference between 2 consecutive moments of the SAN activation: $CL = t_{A+1} - t_A$, where t_A is the activation time of the first LC within the SAN to depolarize during an action potential propagation under consideration and t_{A+1} is during the next action potential propagation.

Relative lifetime of LC is calculated by using the following expression:

$$\rho_i = \frac{\sum_n \delta_{i,n} \cdot CL_n}{\sum_n CL_n} \cdot 100\%, \text{ where } \delta_{i,n} = \begin{cases} 1, \text{if the cell is a LC during } n\text{th SAN activation} \\ 0, \text{otherwise} \end{cases} \tag{8}$$

That is, the numerator of the time ith cell was an LC and the denominator stands for the total time of simulation. This is a dimensionless measure of the LC lifetime at a particular point.

Conduction velocities are calculated via a finite difference technique[37]:

$$CV = \frac{1}{|\nabla t_{E=-30\ mV}|} \tag{9}$$

where $\nabla t_{E=-30\ mV}$ is a local activation time gradient.

Mean conduction velocity (CV) values at a given distance from the center of the SAN were calculated as a mean value within a 0.14-mm-wide annulus.

3 | RESULTS

3.1 | Activation sequence

To reveal the effects of fibroblasts, we compared the results of simulations in the absence and in the presence of fibroblasts. In the absence of fibroblasts, all cells within the SAN (Figure 2, inside the dashed line) depolarized during first 7.9 ms (Figure 2A). In 10 seconds, a number of LCs established, located predominantly from 1.3 to 3.4 mm from the SAN center (Figure 2B and C). Action potential initiated and propagated radially from these LCs. After ACh application at $t = 60$ seconds, the SAN failed to activate atrial tissue: Subthreshold depolarizations were observed in atrial tissue during the first 2 activations of the SAN. Up to $t = 70$ seconds, no new LCs emerged; however, activation sequence changed: LCs that were first to depolarize before ACh superfusion were last to depolarize after ACh superfusion (compare Figure 2B and C to Figure 2E and F).

In the presence of fibroblasts, at early stages, the activation sequence (Figure S1A) looks similar to the one described above (Figure 2A). However, in contrast to the case of the absence of fibroblasts, after a few seconds, LCs shifted toward the SAN center (area within 2 mm from the center of the SAN: Figure S1B and C) from which action potential propagated toward the periphery. Acetylcholine superfusion resulted in LCs shift toward the periphery (Figure S1D-F). Note that, although the activation sequences were different, the locations of LCs were rather close in simulations with and without fibroblasts (Figure S1D-F and 2D-F); at large times, activation maps look almost identical regardless of the presence of fibroblasts (compare Figure S1F with Figure 2F).

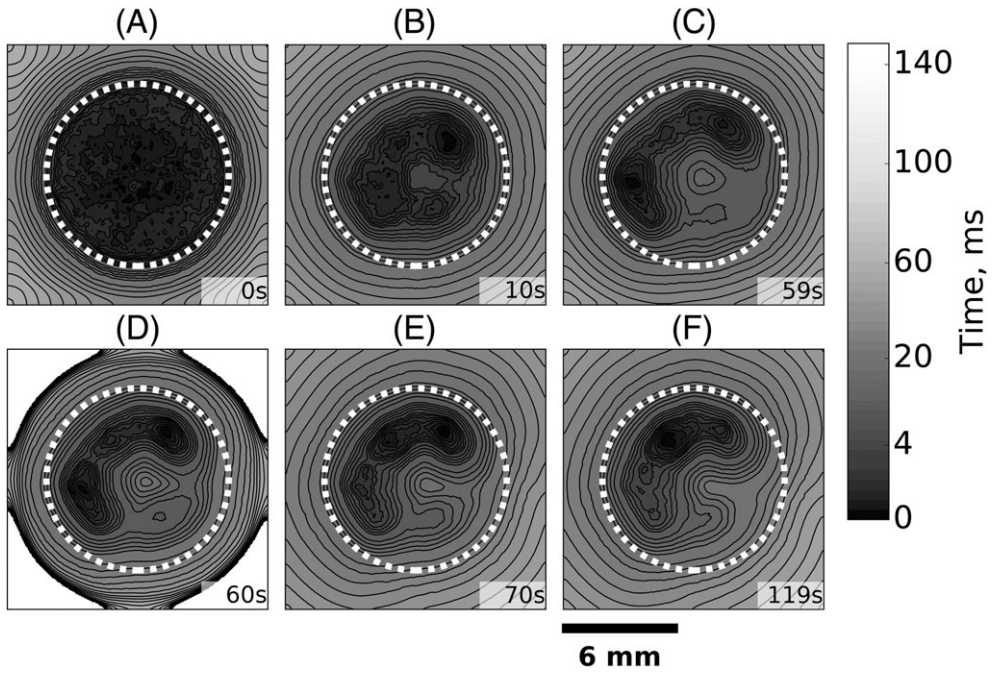

FIGURE 2 Activation maps, no fibroblasts, $P = .0$. Maps at (A) 0.01, (B) 10.21, (C) 59.13, (D) 60.48, (E) 70.03, and (F) 119.34 seconds respectively. Sinoatrial node is inside the dashed line

In heavy fibroblast presence ($P = .6$), the effects became more pronounced: LCs remain in the center of the SAN within a sphere of 1.2-mm radius (Figure 3B and C). After an ACh superfusion, LCs shifted toward the periphery of the SAN; however, their locations (Figure 3D-F) did not coincide with those for $P = .0$ and $P = .4$ cases.

3.2 | Leading center dynamics

Positions of LCs are shown in Figure 4. In the absence of ACh ($t < 60$ s), a rather scattered swarm of LCs is seen for $P = .0$ (Figure 4A). After 4.1 seconds, LCs were located in the range of 1.3 to 3.4 mm from the center. With a moderate presence

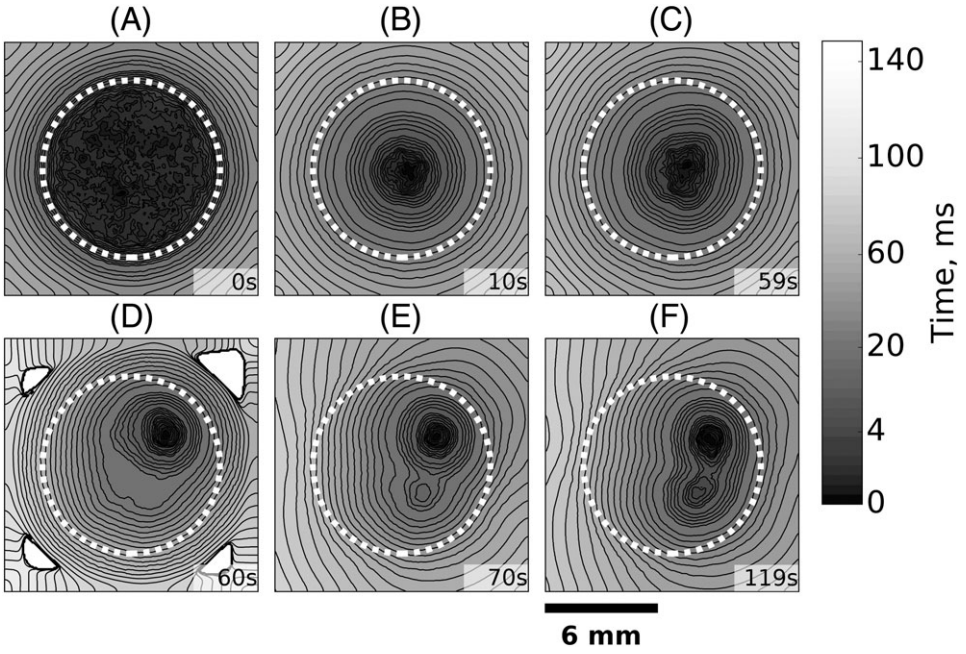

FIGURE 3 Activation maps, heavy fibroblast presence, $P = .6$. Maps at (A) 0.03, (B) 10.22, (C) 59.19, (D) 61.94, (E) 70.33, and (F) 119.32 seconds respectively. Sinoatrial node is inside the dashed line

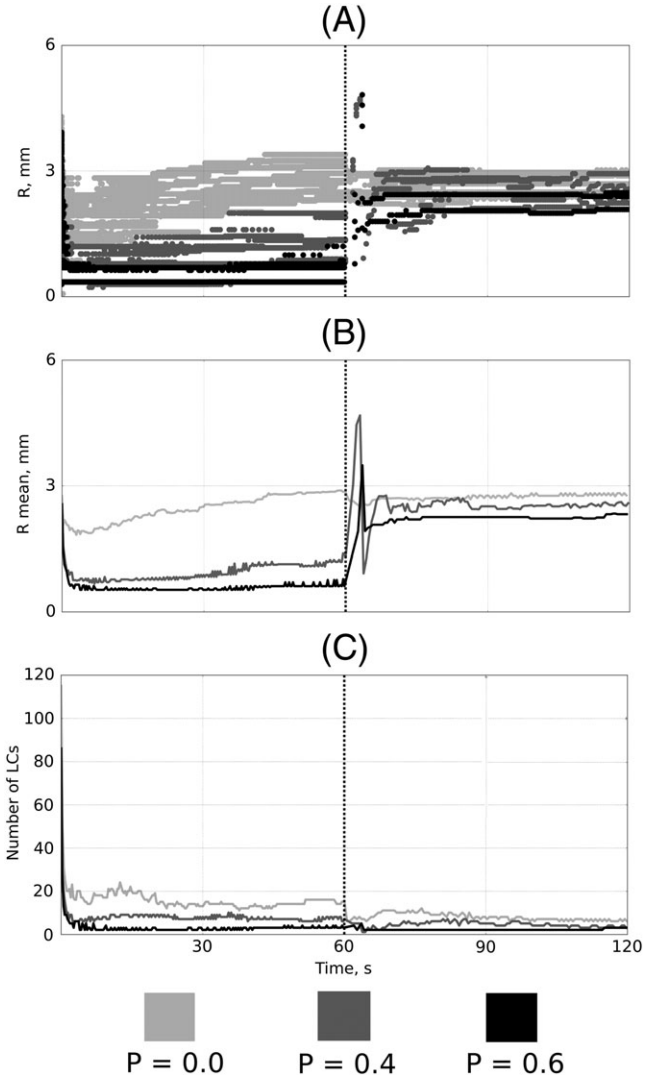

FIGURE 4 Dynamics of leading centers (LCs) in the sinoatrial node (SAN). A, LC distance to the center. Each dot stands for a LC at appropriate time moment. B, LC average distance to the center. C, Number of LCs in the SAN. Acetylcholine was superfused at $t = 60$ seconds (vertical dotted line)

of fibroblasts ($P = .4$), the number of LCs decreased and their locations were in the range 0.2 to 1.2 mm from the center. In heavy presence of fibroblasts ($P = .6$), 2 dominant LCs quickly established, both located at a close distance (0.3 and 0.7 mm) to the center.

After ACh superfusion ($t > 60$ s), LCs located from 1.9 to 3.0 mm from the center regardless of fibroblast-myocyte coupling. Thus, in the presence of ACh, LCs remain in the same area for $P = .0$, while in the presence of fibroblasts, $P > 0$, ACh superfusion resulted in LC shift toward the periphery of the SAN. At $P = .4$, LCs were from 0.4 to 2.0 mm without ACh, from 2.1 to 2.9 mm in the presence of ACh superfusion. At $P = .6$, the LC locations were from 0.3 to 1.2 mm without ACh, from 2.0 to 2.4 mm in the presence of ACh (Figure 4A).

In the absence of ACh ($t < 60$ s), the mean distance of LCs to the center of the SAN, R_{mean}, decreased sharply during the first few seconds followed by a slow gradual increase (Figure 4B). A superfusion of ACh ($t > 60$ s) resulted in violent transient processes ($t = 60$ to 70 s) similar to those described in Syunyaev and Aliev[35] after which LC positions stabilized.

An enormously large amount of LCs in the beginning of simulations (115, 86, and 86 for $P = .0$, .4, and .6 correspondingly) quickly decreased becoming 17, 12, and 5 correspondingly after $t = 20$ seconds (Figure 4C). Acetylcholine superfusion ($t > 60$ s) resulted in further, though not that prominent, decrease in the number of LCs. The effect was the greatest in the case $P = .0$: An ACh application caused a drop in the number of LCs from 15 to 6.

It should be noted that, while just a few LCs are exposed on activation maps (Figures 2, S1, and 3), the computer algorithm does detect numerous ones (up to 115, Figure 4C). However, most of those LCs were short-living transients.

Most LCs generated just a single action potential (Figure 5, small dots) before they died out. Without ACh, a few dominant LCs established quickly in simulations with fibroblasts ($P = .4$ and $P = .6$, large white spots in Figure 5), while lifetime of LCs without fibroblasts was less than 53%. Acetylcholine superfusion increased LC lifetime in the absence of fibroblasts (ie, resulted in the existence of more stable LCs).

3.3 | Conduction velocity

To characterize action potential propagation initiated by LCs, we estimated CV. In all simulated cases, CV reached 70 cm/s and higher in the regions of LC agglomerations, where groups of cells depolarize almost simultaneously, forming a phase-diffusion wave.[38] Initially, a region of phase-diffusion waves occupied most of the SAN except for a narrow ring near the SAN boundary, where CV gradually decreased, demonstrating the mean value of 4.1 ± 0.6 cm/s (Figure 6A). After a few LCs had formed in the tissue, the pattern retained similar: CV was very high in the vicinity of LCs and gradually decreased toward the SAN boundary (the mean value was 5.3 ± 0.4 cm/s near the SAN boundary); however, the region of fast propagation shrank (Figure 6B). High CV was also observed in areas where waves collide with each other (Figure 6C). Acetylcholine superfusion did affect LC locations (and, as a consequence, the distribution of high CV regions) but did not affect the mean CV near the SAN boundary.

In the presence of fibroblasts, the pattern retain similar, but CV in the SAN was slightly smaller; ie, mean CV was very high near the LCs, decreasing to 4.8 ± 0.4 cm/s (Figure S2C) and 4.5 ± 0.4 cm/s (S3C Fig) on the SAN boundary. Acetylcholine superfusion resulted in a slight reduction of the mean CV on the SAN boundary: 4.1 ± 0.4 cm/s (Figure S2F) and 3.8 ± 0.4 cm/s (Figure S3F). Dependence of mean CV versus distance from the center of the SAN for different cases is presented in Figure S4.

3.4 | Chronotropic effects

Surprisingly, fibroblasts hardly affected the CL, unlike in the case of pairs of coupled cells[16]: It was 0.26 second without ACh and 0.49 second after ACh superfusion (Figure 7), except for a short period of transients after $t = 60$ seconds.

An account of fibroblasts in simulations resulted in the phenomenon of a sinus pause: ACh superfusion arrested spontaneous activity of the SAN for 1.9, 1.0, and 0.4 second with $P = .6$, .4, and .2 correspondingly (Figure **7**). Similarly, vagal stimulation initially arrests pacemaking for 1 to 2 seconds in experiments[39,40]; short sinus pauses may be also revealed by Holter monitoring even in healthy subjects.[41] No such effect was observed for $P = .0$, ie, when pacemakers do not interact with fibroblasts. The effect may be caused by intracellular ionic concentration changes, occurring when

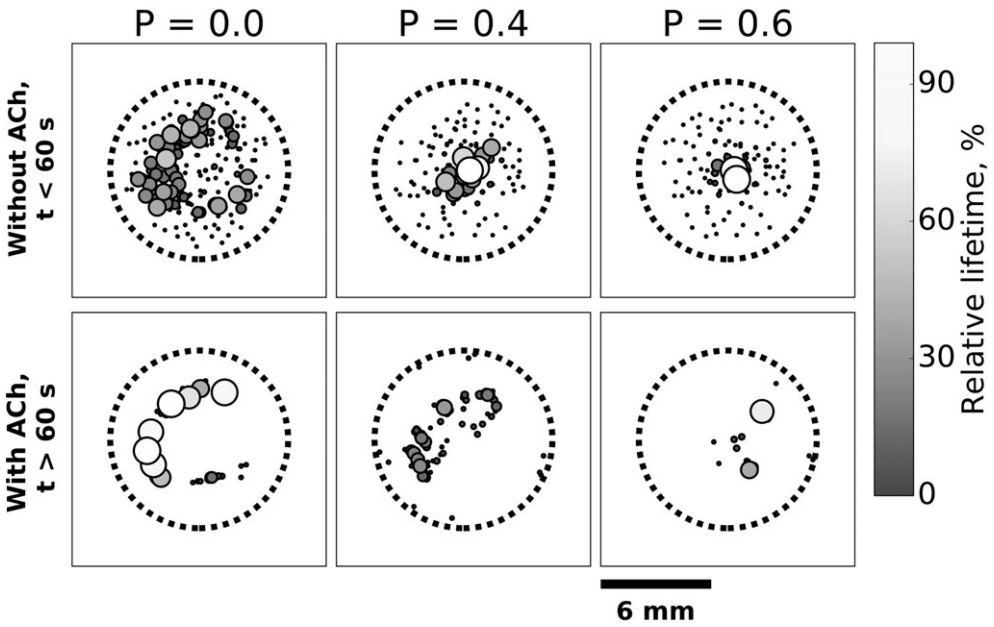

FIGURE 5 Relative lifetimes of leading centers in the sinoatrial node (SAN). A larger lighter spot stands for a greater value; SAN is inside the dashed line

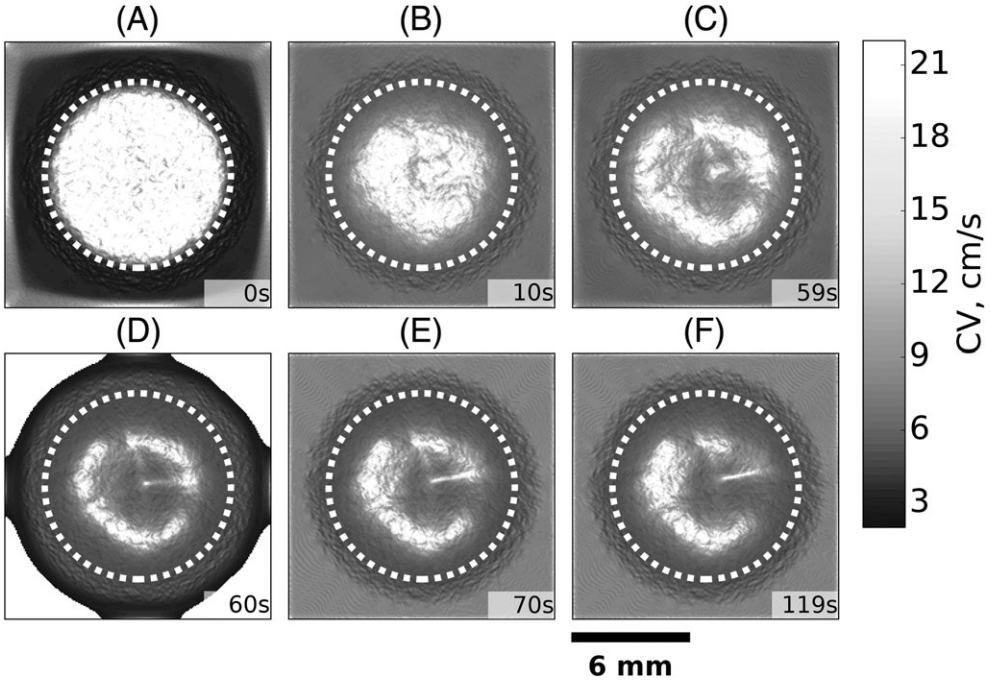

FIGURE 6 A conduction velocity map, $P = .0$. A to F, Correspond to the activation maps in Figure 2; propagation initiated at the moments of 0.01, 10.21, 59.13, 60.48, 70.03, and 119.34 seconds. Sinoatrial node is inside the dashed line

imposed oscillation frequency is different from cells intrinsic frequency as described in Aliev and Chailakhyan.[42] Thus, fibroblasts affect ionic homeostasis in the SAN.

4 | DISCUSSION

4.1 | Major findings

For decades, computer simulations of electrical activity in the SAN were concentrated on effects due to major electrically active fractions of the SAN tissue: SAN pacemaker cells. In this work, we take into consideration fibroblasts, widespread cells in the SAN.[1,2] Our major goal was to study effects of fibroblasts on the rhythm generation and propagation in the SAN. An account of fibroblast-myocyte coupling allowed us to better reproduce experimental results. In particular, we observed propagation from the SAN center, and LCs shift toward periphery (Figures 3 and S1) after ACh superfusion. Fibroblasts are important, because in their absence ($P = .0$), we could see numerous LCs not in the center, but on the SAN periphery, from which action potential propagated toward the SAN center (Figure 2).

It should be noted that experimentally observed LC shifts by millimeters after ACh superfusion[1,27] may be reproduced in simulations ignoring fibroblasts under special conditions of a uniform distribution of central and peripheral cells in the SAN.[4,35] This kind of cell distribution results in numerous LCs, mostly on the SAN periphery[4]; ACh superfusion resulted in LC shift or "migration" by few millimeters. However, a uniform distribution assumes an equal probability to observe both central and peripheral cells everywhere in the SAN, which is less likely to occur in the SAN. If the distribution of cells is nonuniform, and faster-oscillating cells are located on the SAN periphery, then fibroblast-myocyte coupling is required to reproduce the LCs shift toward the SAN periphery after ACh superfusion (Figure 4). One should also note that, while LC location before ACh superfusion heavily depended on the probability of fibroblast-myocyte coupling, after ACh application, distance from LCs to the center of the SAN weakly depends on the model parameters (Figure 4).

The model of the SAN exploited in this work, obviously, includes not all but basic anatomical details and is convenient to study the discussed effects. Simulations performed with the use of a more detailed model of the SAN structure[30] that is based on immunohistochemical studies[31] show similar activation pattern sequence, ie, several LCs on the SAN periphery (Figure 8). This behavior is a consequence of specific cell distribution within the SAN: Intrinsic oscillation frequency of the tissue balls extracted from the SAN periphery is higher than frequency of the SAN center[1] because larger cells from SAN periphery express higher I_f and I_{Na} densities[39,43] compared with small cells in the center.

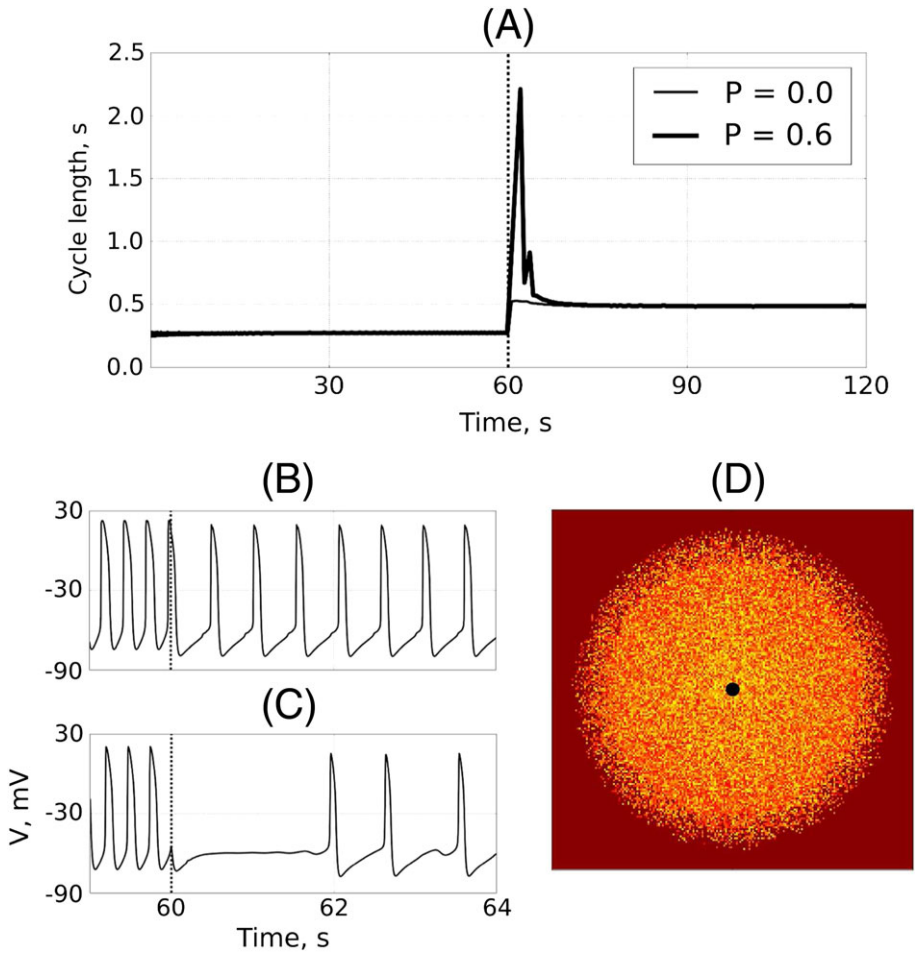

FIGURE 7 Sinoatrial node (SAN) cycle length (A) and action potentials (B and C) at a control point in the center of the SAN. Control point is marked as a thick black dot on (D). No sinus pause for $P = .0$ (B) and a 1.9-second sinus pause for $P = .6$ (C) is seen. Acetylcholine was superfused at $t = 60$ s

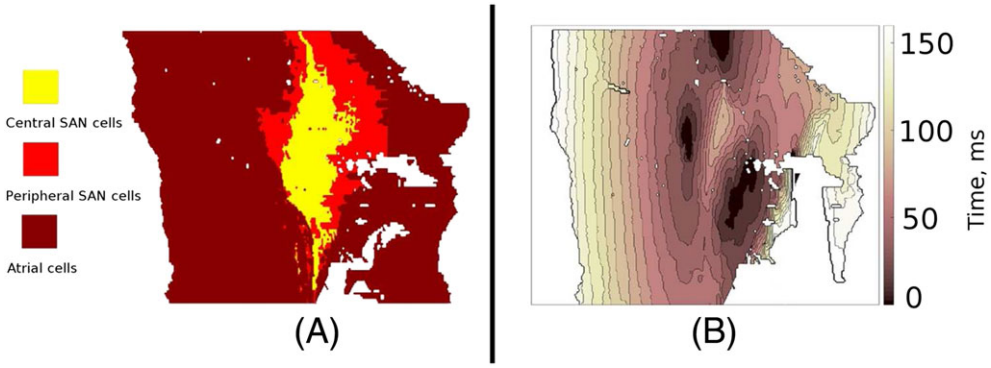

FIGURE 8 A, Anatomically detailed rabbit sinoatrial node (SAN) model, endocardial view. Atrial tissue is tinted brown, peripheral SAN cells tinted red, central SAN cells tinted yellow. B, A sample of an activation sequence. Note a few LCs on the SAN periphery (black areas)

After the transients die out, action potential propagates from the fastest oscillator to slower ones.[29] This contradiction between cell distribution and activation sequence within the SAN tissue had no plausible explanation up to date.

4.2 | Intercellular coupling within the SAN

As mentioned in section 1, an electronic load posed by the atria may shift the LCs toward the SAN center. This was confirmed in simulations with both uniform[4] and nonuniform[5] distributions of cells in the SAN. However, in the latter

case, the effect occurs only if the conductivities in the SAN are very high (150 to 450 nS[5]), while in vitro measurements suggest 0.6 to 25 nS.[6] In vitro cultured cell experiments are likely to underestimate in vivo values, but unlikely by a factor of 10. Here, we show that an account of fibroblasts allows us to observe a shift of LCs toward the center in the case of a nonuniform distribution of cells in the SAN at reasonable conductivities.

An indirect way to estimate intercellular conductance is to measure CV in the SAN. Intercellular conductance in a spontaneously active tissue, which is a system of phase-shifted oscillators, affects CV in a rather indirect way: Despite uniform intercellular conductance within the SAN in our simulations, CV distribution in the SAN is very complex (Figures 6 and S2 and S3). However, it does affect phase shifts between interacting cells,[29] which, in turn, affects the CV in the SAN. Bleeker et al[44] reported the CV within the SAN to be 2 to 8 cm/s, Yamamoto et al[45] reported 3 to 5 cm/s near the SAN center and 30 to 60 cm/s near the SAN periphery.

We observed very high CV around LCs (compare Figures 6 and S2 and S3 with Figures 2, S1, and 3 correspondingly): Local CV in the SAN calculated as activation time gradient was over 70 cm/s, while, for example, the mean CV within 0.5 mm from the center of the SAN in Figure S3C was 26 cm/s. This is a consequence of almost simultaneous depolarization of groups of neighboring cells: Indeed, when local activation time gradients tend to zero, CV tends to infinity. Toward the SAN boundary, CV decreased monotonically down to 3 to 6 cm/s. Because the CV in the SAN was above 3 cm/s, arguably, we can draw a conclusion that intercellular conductance used in simulations is not lower than conductance in central SAN in vivo. Recent human SAN experiments[46] demonstrate similar CV value distribution: 10 to 15 cm/s in the center of the SAN decreased to 6.8 cm/s at the periphery.

4.3 | SAN cell distribution

In simulations, we intentionally used the same distribution of cells. Although exact activation sequence is dependent on the cell distribution, the major conclusions retain: Action potential is initiated in the central part of the SAN, ACh superfusion results in LCs shift toward periphery only if fibroblast-myocyte coupling is taken into account, and fibroblast-myocyte coupling has no effect on the SAN frequency. The conclusions are illustrated in simulations with different myocyte and fibroblasts distributions (Figures S5 and S6).

4.4 | Fibroblast effect on activation sequence: A plausible explanation

As was described previously,[29] interaction of SAN cells with different inherent frequencies results in synchronization of their oscillations. The established CL in the system is close but not equal to the faster-oscillating cell (peripheral SAN) CL, and the faster-oscillating cell is first to depolarize. The distribution of the SAN cells was the same in the simulations presented above, while fibroblasts' effect on peripheral SAN cell action potential is minimal.[16] As a consequence, we did not observe any significant effect of fibroblasts on the frequency of the SAN.

Then, why did fibroblasts affect the activation sequence? The logic is as follows: Fibroblasts are small cells with the membrane capacitance of 6.3 pF as measured in ventricular fibroblasts.[47] The resting membrane potential of fibroblasts is high: −20 to −40 mV.[26,48] In comparison, SAN cells are larger, with 20-pF capacitance of central and 60 pF of peripheral cells.[39] In the simulations, we observed that 2 fibroblasts are enough to suppress spontaneous activity of a central SAN cell[16] and to establish the potential of $V_{rs} = -44$ mV in the system of these coupled cells. This value, V_{rs}, is an analogue of a "resting potential" for this system of coupled cells. On the other hand, 4 fibroblasts attached to a peripheral SAN cell resulted in just a 3% change of its CL.[16] This unequal effect of fibroblasts on SAN cells actually stands behind the effects described above.

To illustrate the said, Figure 9 presents a comparison of action potential in 2 small systems: (i) A cell of a peripheral type is interacting with cells of central type, which, in turn, are coupled to fibroblasts (this pattern is common in the center of the SAN) and (ii) a system of interacting peripheral cells coupled to fibroblasts (this pattern is common in the SAN periphery). In the first case, a cell of peripheral type (per in Figure 9A) interacts with the pacemaker-fibroblast system (Ctr in Figure 9A) with a "resting potential" of $V_{rs} = -44$ mV. This interaction results in a less negative maximum diastolic potential and faster repolarization of a peripheral type cell (Figure 9C). Resulting CL in the first system (Figure 9A) is 6% shorter then CL in the second system (Figure 9B). Thus, little CL change proved to be enough to shift LCs toward the SAN center but is not enough to noticeably affect the SAN frequency.

Note that, although both action potentials in Figure 9C were recorded from the cell of a peripheral type, their waveforms are different. While in the latter case (Figure 9B) one can see typical peripheral cell waveforms, in the first case (Figure 9A), the action potential looks like that of a central SAN cell: less rapid upstroke, more positive takeoff

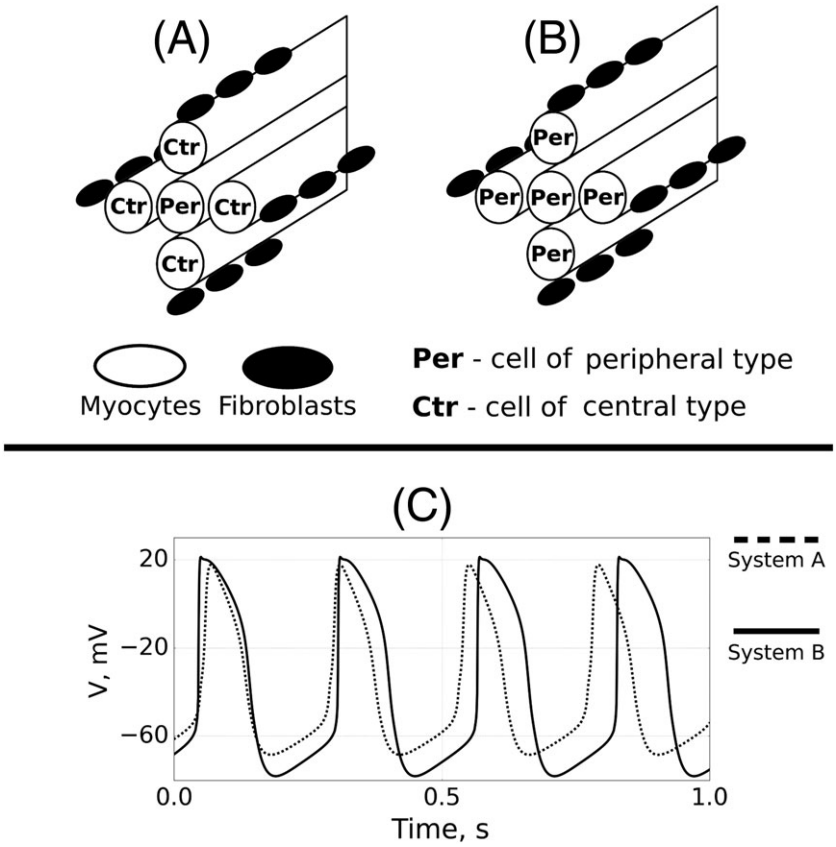

FIGURE 9 On the explanation of activation sequence. A, A cluster composed of a sinoatrial node cell of a peripheral type coupled to cells of central type, which, in turn, coupled to fibroblasts (small black cells). B, A cluster composed of peripheral cells coupled to fibroblasts. C, Action potentials recorded from the middle cell in clusters (A) (dashed line) and (B) (solid line)

potential, and smaller amplitude. The conclusion is that, in the highly heterogeneous tissue of the SAN microelectrode, action potential recordings do not always tell us much about actual cell type.

4.5 | Previous computational studies

Simulations of fibroblasts coupled with a single myocyte have been reported by Greisas and Zlochiver.[49] They show that the CL of a myocite depends nonmonotonically on number of fibroblasts attached to it: A small number of fibroblasts shorten (the effect also reported in Tolstokorov et al[16]), while large number of fibroblasts may prolong the CL. Tissue simulations by Oren and Clancy[50] show that a heterogeneous SAN model that accounts for the difference between central and peripheral SAN cells fails to reproduce a physiological activation sequence. They also studied the effect of fibroblasts on conduction time and CL, simulating fibroblasts with a passive electrical model and assuming that fibroblasts are distributed within a few "islands" in the tissue.[50] The results of our simulations agree in general with these works: We observed decrease of the CL in single-myocyte simulations (Figure 9). We observed that, in a heterogeneous SAN model, the effect of atrial cells is not strong enough to shift LCs to the central part of the SAN. However, in contrast to a passive model, the detailed active model of fibroblasts resulted in pronounce effects on LC dynamics (Figure 4). We argue that interaction of myocytes with fibroblasts may explain a natural activation sequence in the SAN.

4.6 | Model limitations

A few simplifications were used in simulations: All cardiomyocytes were assumed 70 μm long, and intercellular conductance within the SAN was uniform. The simplifications helped us to analyze complex patterns of excitation propagation in the SAN. An additional reason for the simplifications is a lack of unambiguous reliable data on the tissue structure as well as CV and action potential waveform distributions in the SAN. This did not allow us to go into more detail to simulate a particular heart sample. For the same reason, we did not consider particular myocardial fiber orientation within the SAN. Fiber orientations may be important in the case of human, where SAN interacts with atria via separate exit pathways[51]; however, in the case of rabbit SAN, cells form rather irregular mesh[31] as mentioned above.

The main conclusions of this study are limited to the following: (1) A heterogeneous SAN model fails to reproduce propagation from the center of the SAN (in agreement with simulations by previous researchers[5,50]) and (2) fibroblasts electrically coupled to the SAN cells may reverse activation sequence and, consequently, explain why action potential propagates from the center of the SAN.

We also did not account for interaction between fibroblasts. According to Camelliti et al,[11] SAN fibroblasts express Cx40, underlying fibroblast-fibroblast coupling, in fibroblast rich areas and Cx45, underlying fibroblast-myocyte coupling, in myocyte-rich areas. We simulated only the latter: the load caused by fibroblasts on SAN cells and not the conduction through fibroblast-rich "islands." For this reason, we used a 2-layer model in this work: a layer of fibroblasts over a layer of cardiomyocytes. This approach is more natural to reproduce the case of a number of small cells modulating SAN cell activity. On the other hand, to simulate the specifics of propagation obstruction by fibroblast-rich areas, a single-layer model where fibroblasts are incorporated into the myocytes lattice may be more appropriate (eg, as in Oren et al[50]).

5 | CONCLUSIONS

Despite scarce experimental evidence on fibroblast-myocyte coupling in vivo, we believe that this study sheds some light on the problem of action potential initiation and propagation in the SAN. In particular, we attempted to answer the question on how LCs emerge in the central part of the SAN while it is dominated by smaller and slower cells. We hypothesize that some fibroblast-rich regions within the SAN may actually modulate and even reverse activation sequence.

There are many unanswered questions and still awaiting for experimental exploration though. Do fibroblasts couple to central as well as to peripheral SAN cells? Do fibroblast-myocyte couples form a uniform distribution, or are there any fibroblast-rich areas within the SAN? Finally, fibroblast-myocyte coupling in vivo was shown only in the rabbit SAN so far—is it common among different species? We hope that this work may spur further experimental and theoretical studies on the subject that may finally help to understand the principles of the SAN activation. R.A.S. thanks RFBR No. 18-07-01480 for support.

ORCID


Rubin R. Aliev http://orcid.org/0000-0003-3102-3769

REFERENCES

1. Boyett MR, Honjo H, Kodama I. The sinoatrial node, a heterogeneous pacemaker structure. *Cardiovasc Res*. 2000;47(4):658-687. https://doi.org/10.1016/S0008-6363(00)00135-8
2. Opthof T. The mammalian sinoatrial node. *Cardiovasc Drugs Ther*. 1988;1(6):573-597. https://doi.org/10.1007/BF02125744
3. Joyner RW, Kumar R, Golod DA, et al. Electrical interactions between a rabbit atrial cell and a nodal cell model. *AJP-Heart*. 1998;274(6):H2152-H2162.
4. Syunyaev RA, Aliev RR. Computer simulation of 3D electrical activity in the sinoatrial node. *Russian J Num Anal Math Model*. 2011;26(6):575-587. https://doi.org/10.1515/rjnamm.2011.034
5. Garny A, Kohl P, Hunter PJ, Boyett MR, Noble D. One-dimensional rabbit sinoatrial node models: benefits and limitations. *J Cardiovasc Electrophysiol*. 2003;14(10):S121-S132. https://doi.org/10.1046/j.1540.8167.90301.x
6. Verheule S, van Kempen MJ, Postma S, Rook MB, Jongsma HJ. Gap junctions in the rabbit sinoatrial node. *AJP Heart*. 2001;280(5):H2103-H2115.
7. Mangoni ME, Nargeot J. Genesis and regulation of the heart automaticity. *Physiol Rev*. 2008;88(3):919-982. https://doi.org/10.1152/physrev.00018.2007
8. Camelliti P, Borg TK, Kohl P. Structural and functional characterisation of cardiac fibroblasts. *Cardiovasc Res*. 2005;65(1):40-51.
9. Davies MJ, Pomerance A. Quantitative study of ageing changes in the human sinoatrial node and internodal tracts. *Br Heart J*. 1972;34(2):150-152.
10. Shiraishi I, Takamatsu T, Minamikawa T, Onouchi Z, Fujita S. Quantitative histological analysis of the human sinoatrial node during growth and aging. *Circulation*. 1992;85(6):2176-2184.
11. Camelliti P, Green CR, LeGrice I, Kohl P. Fibroblast network in rabbit sinoatrial node: structural and functional identification of homogeneous and heterogeneous cell coupling. *Circ Res*. 2004;94(6):828-835. https://doi.org/10.1161/01.RES.0000122382.19400.14

12. Kohl P, Camelliti P, Burton FL, Smith GL. Electrical coupling of fibroblasts and myocytes: relevance for cardiac propagation. *J Electrocardiol*. 2005;38(4 Suppl):45-50.

13. Ongstad EL, Gourdie RG. Myocyte-fibroblast electrical coupling: the basis of a stable relationship? *Cardiovasc Res*. 2012;93(2):215-217. https://doi.org/10.1093/cvr/cvr338

14. Vasquez C, Benamer N, Morley GE. The cardiac fibroblast: functional and electrophysiological considerations in healthy and diseased hearts. *J Cardiovasc Pharmacol*. 2012;57(4):380-388. https://doi.org/10.1097/FJC.0b013e31820cda19

15. Goldsmith EC, Hoffman A, Morales MO, et al. Organization of fibroblasts in the heart. *Dev Dyn*. 2004;230(4):787-794.

16. Tolstokorov AS, Syunyaev RA, Aliev RR. Simulation of the fibroblast effect on electrical activity of sinoatrial node cells. *Biophysics*. 2015;60(2):256-262.

17. Aliev RR, Chailakhyan LM. Study of the effect of acetylcholine on intracellular homeostasis of true pacemaker cells of rabbit sinus node using computer simulation. *Dokl Biochem Biophys*. 2005;402(1):236-239.

18. Aliev RR, Fedorov VV, Rosenshtrakh LV. Simulation of ACh effects on ionic current of primary and subsidiary pacemakers single cells of rabbit sinoatrial node. *Dokl Biol Sci*. 2004;397(5):697-700.

19. Aliev RR, Fedorov VV, Rosenshtrakh LV. Study of the effect of acetylcholine on the excitability of true pacemaker cells of rabbit sinus node using computer simulation. *Dokl Biol Sci*. 2005;402(4):548-550.

20. Zhang H, Holden AV, Kodama I, et al. Mathematical models of action potentials in the periphery and center of the rabbit sinoatrial node. *AJP Heart*. 2000;279(1):H397-H421.

21. Zhang H, Holden AV, Noble D, Boyett MR. Analysis of the chronotropic effect of acetylcholine on sinoatrial node cells. *J Cardiovasc Electrophysiol*. 2002;13(5):465-474. https://doi.org/10.1046/j.1540-8167.2002.00465.x

22. Aliev RR. *Conceptual and Detailed Models of Electrical Activity of the Myocardium*. Saarbrucken, Germany: Lambert Academic Publishing; 2012. ISBN:978-3-8465-3943-9 (in Russian).

23. Lindblad DS, Murphey CR, Clark JW, Giles WR. A model of the action potential and underlying membrane currents in a rabbit atrial cell. *AJP Heart*. 1996;271(4):H1666-H1696.

24. MacCannell KA, Bazzazi H, Chilton L, Shibukawa Y, Clark RB, Giles WR. A mathematical model of electrotonic interactions between ventricular myocytes and fibroblasts. *Biophys J*. 2007;92(11):4121-4132.

25. Verheule S, Van Kempen MJ, Te Welscher PH, Kwak BR, Jongsma HJ. Characterization of gap junction channels in adult rabbit atrial and ventricular myocardium. *Circ Res*. 1997;80(5):673-681.

26. Rook MB, van Ginneken AC, de Jonge B, el Aoumari A, Gros D, Jongsma HJ. Differences in gap junction channels between cardiac myocytes, fibroblasts, and heterologous pairs. *AJP Cell Physiol*. 1992;263(5 Pt 1):C959-C977.

27. Abramochkin DV, Kuzmin VS, Sukhova GS, Rosenshtraukh LV. Modulation of rabbit sinoatrial node activation sequence by acetylcholine and isoproterenol investigated with optical mapping technique. *Acta Physiologica*. 2009;196:385-394. https://doi.org/10.1111/j.1748-1716.2009.01963.x

28. Boyett MR, Kodama I, Honjo H, Arai A, Suzuki R, Toyama J. Ionic basis of the chronotropic effect of acetylcholine on the rabbit sinoatrial node. *Cardiovasc Res*. 1995;29(6):867-878. https://doi.org/10.1016/S0008-6363(96)88625-1

29. Syunyaev RA, Aliev RR. Modelling of the influence of gap-junction coupling on synchronization of central and peripheral sinoatrial node cells. *Biophysics*. 2009;54(1):58-60. https://doi.org/10.1134/S0006350909010102

30. Syunyaev RA, Aliev RR. Computer simulations of reentrant activity in the rabbit sinoatrial node. *Int J Num Meth Biomed Eng*. 2016;33(2). https://doi.org/10.1002/cnm.2792

31. Dobrzynski H, Li J, Tellez J, et al. Computer three-dimensional reconstruction of the sinoatrial node. *Circulation*. 2005;111(8):846-854. https://doi.org/10.1161/CIRCRESAHA.108.172403

32. Xie Y, Garfinkel A, Camelliti P, Kohl P, Weiss JN, Qu Z. Effects of fibroblast-myocyte coupling on cardiac conduction and vulnerability to reentry: a computational study. *Heart Rhythm*. 2009;6(11):1641-1649. https://doi.org/10.1016/j.hrthm.2009.08.003

33. Fedorov VV, Hucker WJ, Dobrzynski H, Rosenshtraukh LV, Efimov IR. Postganglionic nerve stimulation induces temporal inhibition of excitability in rabbit sinoatrial node. *Am J Physiol Heart Circ Physiol*. 2006;291(2):H612-H623. https://doi.org/10.1152/ajpheart.00022.2006

34. Roberts LA, Slocum GR, Riley DA. Morphological study of the innervation pattern of the rabbit sinoatrial node. *Am J Anat*. 185(1):74-88. https://doi.org/10.1002/aja.1001850108

35. Syunyaev RA, Aliev RR. Computer simulations of pacemaker shift in the sinoatrial node. *Biophysics*. 2010;55(6):1132-1137.

36. Rush S, Larsen H. A practical algorithm for solving dynamic membrane equations. *IEEE Trans Biomed Eng*. 1978;25(4):389-392.

37. Cantwell CD, Roney CH, Ng FS, Siggers JH, Sherwin SJ, Peters NS. Techniques for automated local activation time annotation and conduction velocity estimation in cardiac mapping. *Comput Biol Med*. 2015;65:229-242. https://doi.org/10.1016/j.compbiomed.2015.04.027

38. Syunyaev RA, Aliev RR. Action potential propagation and phase dynamics in the sinoatrial node. *Russian J Num Anal Math Model*. 2012;27(5):493-506. https://doi.org/10.1515/rnam-2012-0028

39. Kodama I, Nikmaram MR, Boyett MR, Suzuki R, Honjo H, Owen JM. Regional differences in the role of the Ca^{++} and Na^{+} currents in pacemaker activity in the sinoatrial node. *AJP Heart*. 1997;272:H2793-H2806.
40. Shibata N, Inada S, Mitsui K, et al. Pacemaker shift in the rabbit sinoatrial node in response to vagal nerve stimulation. *Exp Physiol*. 2001;86(2):177-184.
41. Mølgaard H, Sørensen KE, Bjerregaard P. Minimal heart rates and longest pauses in healthy adult subjects on two occasions eight years apart. *Eur Heart J*. Aug 1989;10(8):758-764. https://doi.org/10.1093/oxfordjournals.eurheartj.a059561
42. Aliev RR, Chailakhyan LM. Study of the preautomatic pause under exposure to acetylcholine in true pacemaker cells of rabbit sinus node using computer simulation. *Dokl Biochem Biophys*. 2005 May-Jun;402(1-6):251-253.
43. Honjo H, Boyett MR, Kodama I, Toyama J. Correlation between electrical activity and the size of rabbit sino-atrial node cells. *J Physiol*. 1996;496(Pt 3):795-808.
44. Bleeker WK, Mackaay AJC, Masson-Pevet M, Bouman LN, Becker AE. Functional and morphological organization of the rabbit sinus node. *Circ Res*. 1980;46(1):11-22.
45. Yamamoto M, Honjo H, Niwa R, Kodama I. Low frequency extracellular potentials recorded from the sinoatrial node. *Cardiovasc Res*. 1998;39(2):360-372.
46. Csepe TA, Zhao J, Hansen BJ, et al. Human sinoatrial node structure: 3D microanatomy of sinoatrial conduction pathways. *Prog Biophys Mol Biol*. 2016;120(1-3):164-178. https://doi.org/10.1016/j.pbiomolbio.2015.12.011
47. Chilton L, Ohya S, Freed D, et al. K+ currents regulate the resting membrane potential, proliferation, and contractile responses in ventricular fibroblasts and myofibroblasts. *AJP Heart*. 2005;288(6):H2931-H2939. https://doi.org/10.1152/ajpheart.01220.2004
48. Kamkin A, Kiseleva I, Isenberg G. Activation and inactivation of a non-selective cation conductance by local mechanical deformation of acutely isolated cardiac fibroblasts. *Cardiovasc Res*. 2003;57(3):793-803.
49. Greisas A and Zlochiver S, "Modulation of cardiac pacemaker inter beat intervals by sinoatrial fibroblasts—A numerical study," 2016 38th Annual International Conference of the IEEE Engineering in Medicine and Biology Society (EMBC), Orlando, FL, 2016, pp. 165-168. doi: https://doi.org/10.1109/EMBC.2016.7590666
50. Oren RV, Clancy CE. Determinants of heterogeneity, excitation and conduction in the sinoatrial node: a model study. *PLoS Comput Biol*. 2010;6(12):e1001041. https://doi.org/10.1371/journal.pcbi.1001041
51. Efimov IR, Fedorov VV, Joung B, Lin SF. Mapping cardiac pacemaker circuits: methodological puzzles of the sinoatrial node optical mapping. *Circ Res* 2010;106(2):255–271. Epub 2010/02/06. pmid:20133911; PubMed Central PMCID: PMC2818830

SUPPORTING INFORMATION

Additional Supporting Information may be found online in the supporting information tab for this article.

How to cite this article: Karpaev AA, Syunyaev RA, Aliev RR. Effects of fibroblast-myocyte coupling on the sinoatrial node activity: A computational study. *Int J Numer Meth Biomed Engng*. 2018;34:e2966. https://doi.org/10.1002/cnm.2966